Original Article

Degradation Assessment of Oil-Impregnated Paper Insulation for Converter Transformer Based on FDS using Digital Image Processing

Shrikant S. Mopari[1], D. S. More[2], A. S. Bhalchandra[3], Pannala Krishna Murthy[4], K. M. Jadhav[5]

[1,2]*Department of Electrical Engineering, Walchand College of Engineering, Sangli, India.*
[3]*Department of Electronics Engineering, Government College of Engineering, Aurangabad, India*
[4]*Department of Electrical Engineering, Sri Chaitanya Institute of Technology & Research, Khammam, India.*
[5]*University Department of Basic and Applied Sciences, MGM University, Aurangabad, Maharashtra, India.*

[1]*Corresponding Author : mopari1977@gmail.com*

Abstract - The Oil-Impregnated Paper (OIP) insulation is commonly utilized as the foremost insulation type in the case of a converter transformer, which is constantly and unavoidably affected by elevated temperature and different stresses arising during the mode of operation. It causes a safety risk to the insulation system of the converter transformer. Because of this, the present study examines the effect on OIP insulation using the FDS technique as a function of frequency and elevated temperature. The Frequency Domain Spectroscopy (FDS) and Atomic Force Microscopy (AFM) techniques were carried out for condition evaluation and surface morphological changes of OIP insulation. The experimental results show that elevated temperature viz 30°C, 50°C, 70°C, 90°C, 110°C and 130°C produces irreversible damage to the surface of OIP, which can lead to morphological changes. The frequency-dependent permittivity studies also confirm the deterioration of OIP insulation as permittivity decreases with increased frequency. However, the synergistic effect generated on the OIP insulation can also be analyzed by image processing-based evaluation methods dependent on the average of four local areas of AFM images. One disk of a valve side star winding single phase converter transformer is developed in MATLAB Simulink. An impulse of 20kV, 1.2/50μsec is applied to study the correlation among insulation degradation across the turn by considering elevated temperature and frequency dependence of OIP insulating material by wavelet transform. The energy of the wavelet coefficient is utilized to analyze the insulation degradation of insulation of the converter transformer. Thus the effectiveness of the FDS study revealed the condition monitoring of converter transformer insulation, and the presented results agree with the published work.

Keywords - Atomic Force Microscopy, Converter transformer, Elevated temperature, Frequency Domain Spectroscopy, Oil Impregnated Paper, Wavelet transform.

1. Introduction

The converter transformer performs a dynamic task in an electrical power system's transmission and distribution network. The converter transformer insulation weakens when subjected to harsh operating conditions. The transformer insulating system mainly consists of Oil-Impregnated Paper (OIP). The transformer oil acts as insulation as well as coolant. The primary constituent OIP insulation is a polymer of glucose and Cellulose which degrades because of the stresses and elevated temperature during the operation.

The reliable performance and avoiding the transformer outage depends upon the insulating material's character. Thus, insulation degradation due to thermal ageing is recognized as a prime cause of transformer failure. Hence to ensure reliable and safe operation performance, there is a need to test transformer insulation regularly.

Thus, DGA analysis is regularly used to diagnose oil and thermally degraded insulating paper [1, 29], but methods produce certain limitations for the actual status of insulating cellulose paper. Due to the above reasons, utility engineers are more interested in non-invasive methods to examine transformer cellulose insulation.

During the 1990s, Return Voltage Measurement (RVM) [3, 34] and Polarization and Depolarization Current (PDC) techniques [4-5] were the most widely popular to measure insulation conditions. RVM is a non-destructive technique with certain limitations for separately assessing oil and paper

insulation conditions. PDC measurement can overcome this limitation without opening the tank for paper sampling. However, examining the influence of ageing products and their effect on PDC measurements is not easy.

On the other hand, the FDS technique is more appropriate for on-site insulation diagnosis, with abundant insulation information and powerful anti-interference capacity. The FDS technique involves using a sinusoidal electrical field with variable frequency. Other non-destructive diagnostic tools like X-Ray Diffraction (XRD), Scanning Electron Microscopy (SEM), and Atomic Force Microscopy (AFM) are also used to study the microstructural deterioration of the OIP insulation under the thermal ageing mechanism. Many researchers have investigated insulation characteristics utilizing D.P. and SEM images under controlled laboratory conditions. During a low-frequency region, a significant impact of thermal ageing on the FDS test is recorded [6-8]. Some corrective measures are suggested for insulation diagnosis but fail to discuss problems associated with parameter variation [11].

The thermally aged pressboard insulation can be analyzed utilizing activation energy based on frequency-temperature shift factor α_T [12].E. I. Koufakiset. al. [14] determine the thermal lifetime of insulating material utilizing the thermal Coefficient in a distribution transformer. The researcher [15] derived an enhanced model based on the Kinetic specification of thermal degradation cellulose. Recently, thermal insulation monitoring and FFT analysis have been used for insulation degradation analysis [16]. The percentage of moisture variation, ageing product, and ageing of pressboard samples significantly impacted FDS test results. The literature found that among the above ageing products plus the pressboard, ageing significantly influences FDS data compared to moisture but fails to discriminate it effectively [18-19].

The moisture and ageing effect can be discriminated by extracting a grouping of feature parameters from the dielectric loss tangent (tan δ) curve. The tanδ curve is significantly influenced by moisture under medium and high frequency, whereas ageing under low frequency ($10^{-3} < f < 10^{-1}$ Hz) region [21]. Youyuan Wang et al. [22] discriminate based on the imagery part of permittivity ε'', correlating moisture and D.P. value. Currently, moisture impacts are significantly analyzed by exploiting commercial IDA-200 dielectric response analyzers available in the market. [6, 17, 20]

In practice, the performance of OIP insulation is significantly affected by the cumulative effects of repeated impulses and the composite electric field. Many researchers utilize AFM phenomena to identify morphological changes on insulation surfaces and discuss the average, RMS roughness, and statistical parameters [26,

27]. Some researchers have a Composite AC-DC electric field. The maximum voltage of 5.3% reduction with vegetable oil is recorded compared to mineral oil [28]. The composite AC-DC voltage application produced a significant impact as compared to D.C. voltage [29].

Pannala Krishna Murthy et al. [35] presented an investigation on detecting various line faults across HVDC transmission by using wavelet transform. The wavelet coefficient of D.C. voltage is used over D.C. current with 99.3% efficiency for identifying faults. The researcher used the S-transform to analyze non-stationary signals to differentiate internal and external faults.

The high-frequency transient voltage will be attenuated for external faults, and signals will persist untouched for internal faults [36]. Some researchers discriminate faults based on multiresolution wavelet analysis [37] and by comparing polarity features of currents at the end of faulty lines using wavelet transform [38].

The same approach is recorded for power system protection based on a transient current-based micro-grid, using Biorthogonal 1.5 as the mother wavelet, and faults detection and discrimination occur within a half cycle with detail coefficients [39, 40]. The researcher studied various techniques, including the wavelet transforms with Biorthogonal 2.2, as the mother wavelet provides a superior accuracy level for early fault detection [41]. With the same approach, researcher [42] proposed a fault identification algorithm in transformers using wavelet and BPNN with overall efficiency exceeding 95%.

Thus, it is observed that the majority of past investigations are restricted to time domain-based and statistical parameters using the frequency-based FDS method. However, for a more accurate and early prediction of the synergetic effect of elevated temperature, there is a need to use sophisticated image processing-based evaluation techniques. In this paper, the phenomena of frequency and elevated temperature dependence OIP insulation by FDS are marked out, and various measurements and comparisons outline experimental evidence for it.

The AFM observations and statistical parameters, such as average and RMS roughness, etc., indicate morphological changes in the OIP insulation. Both surface roughness and dielectric parameters magnify with applying temperature and frequency. Image processing-based techniques confirm these results. In addition to this, entropy, wavelet coefficient, and energy components also confirm these speculations. The rest of the sections of the manuscript are arranged as under, section 2 presents the experimental setup, results are reviewed in Section 3, analysis of converter transformer insulation degradation using wavelet transform is discussed in Section 4, and Section 5 is related to the conclusion.
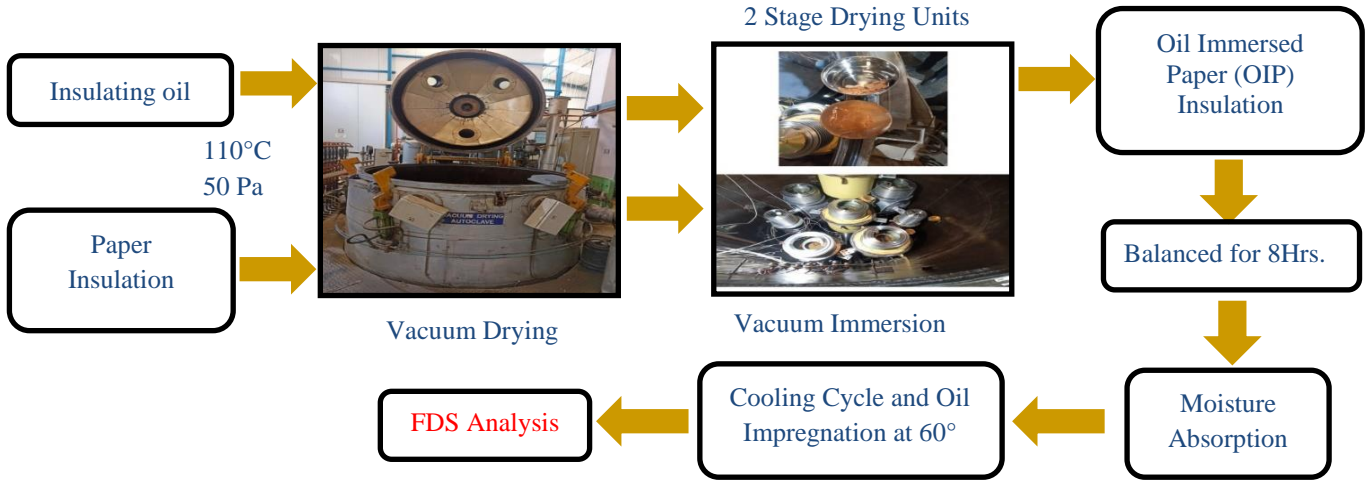
Fig. 1 Flowchart for OIP insulation sample preparation

2. Experimental Details

2.1. Sample Preparation

The samples of paper insulation (10 mm diameter and 0.5mm thickness) were dried at 110 °C for 24 h in the oven under vacuum. Pure mineral oil impregnates the samples again for 24 h using a two-stage drying unit.

A 25-50 mbar vacuum was created and maintained in the oven for eight h to eliminate unwanted moisture from the insulation paper. The above drying process is repeated the second time, in which the temperature was kept at 110 for 8 h, and a vacuum was maintained for 6 h.

The doubly dried paper-insulated samples were slowly cooled to a temperature of 60°C. At this temperature, the paper insulation sample was again oil-impregnated. These oil-impregnated samples were kept in glassware surrounded by a cool, dry, and well-ventilated environment. An experimental setup at Vivid Grid Solutions Ltd., E-106, Waluj MIDC, Aurangabad, was used to prepare Oil-Impregnated Paper (OIP) samples. The different steps involved in oil-impregnated paper insulation samples are illustrated in Figure 1.

2.2. Characterizations

A.C. conductivity, real and imaginary parts of permittivity, and dielectric loss tangent studies on Oil-Impregnated Paper (OIP) samples were carried out as a function of temperatures at 30,50, 70, 90,110, and 130°C and the frequency range of 1 Hz to 10 MHz using PSM 1735, Newtons4th Ltd.

The applied A.C. sinusoidal voltage was 2.5 Volt. The dielectric parameters, such as relative permittivity and dielectric loss, are calculated based on the applied voltage, current, and phase difference. The experimental arrangement is shown in Figure 2.

Fig. 2 Experimental arrangement

The topography of temperature ageing samples was analyzed using AFM images. The AFM instrument of PARK XE-7 was used to collect appropriate insulation images with a scan rate of 0.5 Hz and a scan window size of 3x3 μm. MATLAB R2021b was used for the analysis of the selected image database. Images are pre-processed before analysis, whereas pre-processing includes resizing to 256x256 and converting into a grey scale.

3. Results and Discussions

3.1. Influence of Frequency and Temperature on OIP Insulation

The dielectric parameters were measured to explore further the effect of elevated temperature on the performance of OIP insulation. The measurement of permittivity concerning frequency was carried out for varying elevated temperatures.

Figure 3 illustrates deviation in the fundamental part of permittivity (ε') of OIP samples as a function of frequency at various elevated temperatures. It can be noticed that an increment in frequency causes a decrement in ε'. The decrement in ε' is sharp near the low-frequency region, while at the high-frequency region, the decrement in ε' is very small and almost remains approximately constant; with increasing temperatures, the ε' decreases. The observed variation of ε' can be explained based on the following expression for the fundamental part of relative permittivity.
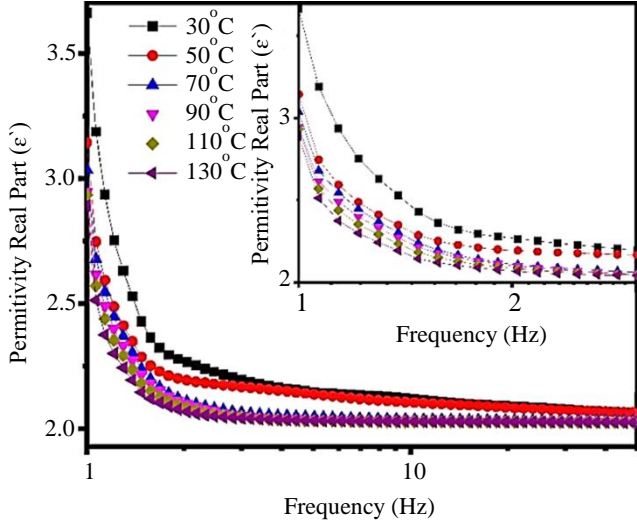
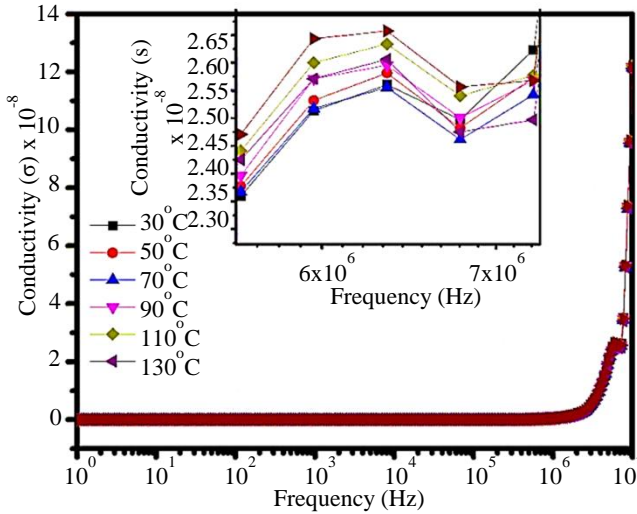**Fig. 3 Real part of permittivity of OIP under different temperatures**

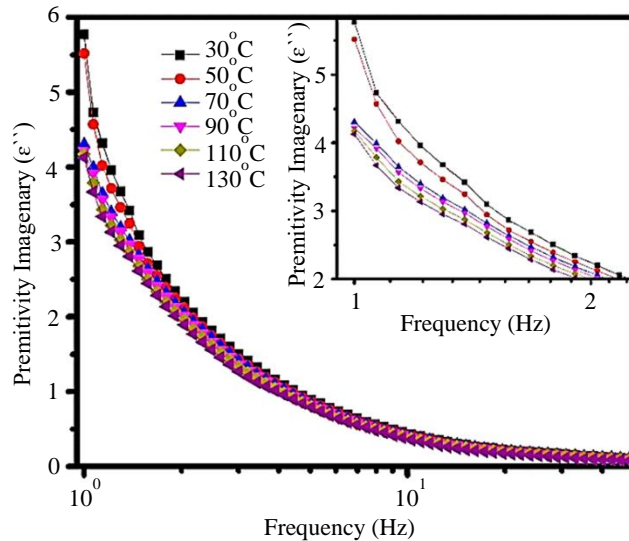

Fig. 4 Conductivity of OIP under different temperatures

Fig. 5 Imaginary part of permittivity (ε") of OIP under different temperatures

$$\varepsilon' = \varepsilon_\infty + \frac{\varepsilon_S - \varepsilon_\infty}{1 + (\omega\tau)^2} \tag{1}$$

Where τ is the time constant of relaxation polarization, ω is the frequency of the electric field, ε_S and ε_∞ are static dielectric constants and optical dielectric constants, respectively, $\varepsilon_S > \varepsilon_\infty$.

The observed behaviour of ε' at low-frequency regions can be attributed to the fact that the relative polarization of the dipoles is fully established due to the sufficient turnaround time. At high-frequency regions, the dipole moment lacks the change in electric field frequency, which results in insufficient polarization dipole, and therefore the value of ε' is around ε∞. It can be further observed from Figure 3 that the permittivity ε' goes on decreasing as temperature increases from 30°C to 130°C.In low-frequency region, the permittivity ε' lie between 3.8 to 2.5. The decrease in permittivity concerning incrementing in temperature is due to the increasing polarization phenomenon as the mobility of the charge carrier increases with temperature.

Figure 4 illustrates the conductivity (σ) trends of OIP as a function of frequency under different temperatures. Moreover, it is found that for the low-frequency range, the σ for OIP also increases when temperature increases. In the case of a dielectric containing m number of charge carriers, the conductivity (σ) can be calculated with equation 2.

$$\sigma = \sum_{i=1}^{m} n_i q_i \mu_i \tag{2}$$

Where n_i is the concentration of the carrier, q_i is the electric charge of the carrier, and μ_i is the carrier's mobility. Under the uniform electric field, the mobility and electric charge are constant for the same carrier. Therefore, the value of σ depends on carrier concentration n_i, which is solely controlled by the number of molecules within the dielectric. Based on equation (2), this increase in σ can be explained by generating short-chain molecules and polar groups due to the succession of cellulose chains and oil molecules due to increased temperature. Thus, it can enhance the polarizing ability of dielectrics and consequently further enhance carrier concentrations. Consequently, the elevated temperature is the key reason for the increase in surface roughness and relative permittivity, as it leads to the creation of polar substances and a change in the fiber structure. Considering the existence of conductivity in the real dielectric, equation (3) can be used to express the relationship between tanδ and ε",

$$\tan\delta = \frac{\sigma/\omega\varepsilon_0 + \varepsilon''_{(\omega)}}{\varepsilon'_{(\omega)}} \tag{3}$$

The ε" and tan(δ) plots of OIP samples under different temperature conditions are shown in Figures 5 and 6. Here ε" decreases and tan(δ) increases with increasing temperature,

particularly in the lower frequency region. As a result, older OIP samples will lose more energy during the polarization processes due to increased relaxation polarization losses, interfacial polarization losses, and conduction losses. In response to the increase in temperature, an increasing number of polar molecules will be created by the covalent bonds breakdown in the cellulose chains in addition to the oil molecules, thereby increasing the concentration of carriers. The increased conductivity causes the conduction loss and tan(δ) to increase. The temperature damage and ageing products cause a drastic change in surface morphology, also dielectric properties of OIP samples due to elevated temperatures.

3.2. FTIR Spectroscopy

The types of bonds present have been studied using FTIR spectroscopy. Thus, it is applied to the quantitative examination of the degradation of by-products on OIP insulation samples. The numbers of stretched and bending vibrations give information about the bonding structure of the OIP sample or degradation of OIP insulation. A sharp, high-intensity characteristic peak in OIP insulation appeared at 2925.64 cm-1, indicating stretching of C-H with changes in the bond's length which is evidence for the presence of methyl group. The peak at 1744.87 cm-1 corresponds to the bending vibration C=O of carbonyl groups present.

In contrast, the peat at 1374.24 cm-1 represents the absorption peak due to alkenes—the low-intensity absorption peak results from the OIP insulation at elevated temperatures. The peak at 726.36 cm-1 represents the out-of-plane bending of C-H. A stretch in C=C has been visualized at 1458.2 cm-1 resulting from aromatic rings at elevated temperatures. Apart from these, a minor peak visible at 1457.29 cm-1 is attributed to ketones groups present. In contrast, the peak corresponding to wave number 721.72 cm-1 may be out-of-plane vibrations or of olefins overlapping or vibration of CH2. Thermal ageing or degradation may result in slight shifts in peak positioning or reduction in peak intensity in the spectrum in OIP insulation. The observed results show that OIP insulation has been degraded with elevated temperature and frequency variation. The spectral analysis displays a distinctive absorbance peak at 2923.01

cm-1 with a high intensity that recognizes the C-H stretch demonstrating alkanes' existence.

3.3. Atomic Force Microscopic Image-based Study

The performance of OIP is significantly related to the impact of temperature on its surface. Micro-damages caused by temperature change are studied with Atomic Force Microscopic (AFM) observations. AFM images at various temperatures are collected for analysis. The temperature is applied to the sample in the range of 30°C to 130°C at the interval of 20°C with a frequency variation from 1Hz to 10 MHz. Four significant local areas around the centre of the sample are randomly chosen and tested under AFM with the assumption that the deterioration is homogenous.

Figure 8(a) shows a virgin OIP sample with a smooth and uniform surface without significant protuberances. Figures 8(b), 8(c), and 8(d) show AFM images of the OIP sample at 90°C, 110°C, and 130°C with significant increments in protuberances as compared to the virgin sample. The surface develops cracks as temperature increases and more prominent protuberances appear. Similarly, in 3D AFM images, it is also observed that there is a notable rise in the degree of fluctuation and fluctuation ratio of a unit area with an increase in temperature.
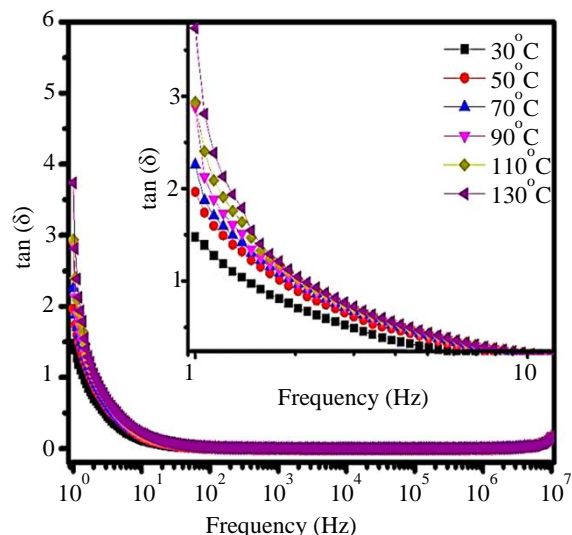

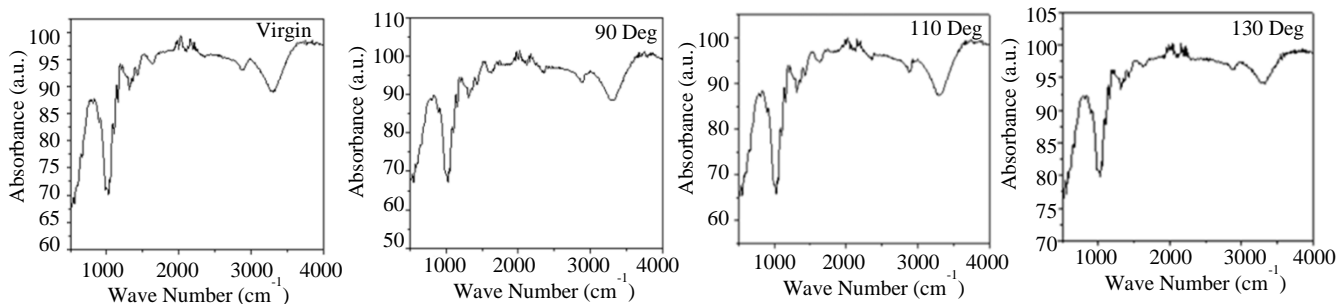**Fig. 6 Tan(δ) of OIP under different temperatures**

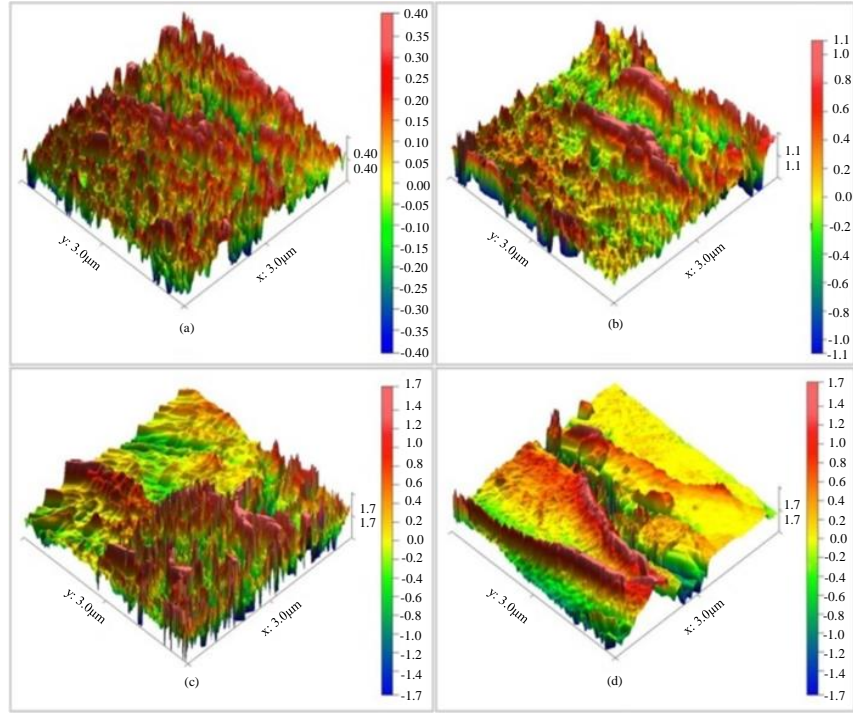**Fig. 7 Bonding analysis using FTIR spectrum**

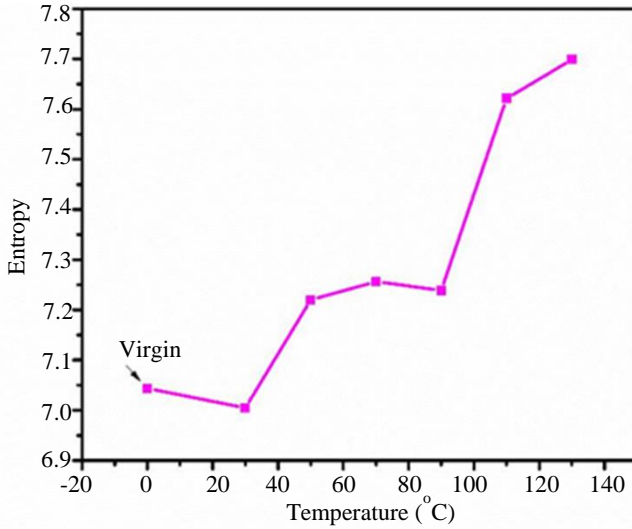**Fig. 8 Topographical images of (a), (b), (c), (d)**

Fig. 9 Temperature vs Entropy

The performance evaluation of AFM images was done using time and frequency domain parameters;

3.3.1. Time Domain Parameters
Texture represents spatial variation in the surface image. The image's texture is generally described as smooth, rough, and bumpy as a function of pixel intensities. Quantification of this parameter is performed by calculating entropy and Energy. As temperature applied to sample paper changes, surface quality. Since it is reflected as a texture in AFM images, as the effect of temperature on sample paper cannot be described only in terms of pixel intensities, Texture

analysis is functional, represented with Time domain parameters, such as entropy, energy, and standard deviation of image and surface roughness.

3.3.2. Frequency Domain Parameters
Wavelet Transform of the image represents spectral information about the AFM image. Discrete Wavelet Transform (DWT) is used to analyze images indicating the effect of ageing on insulation.

3.3.3. Entropy
Entropy meant intensity distribution or homogeneity of the image structure. To determine the effect of temperature on samples, the texture is calculated in terms of the Entropy of AFM images [31,32]. Figure 9 represents entropy v_s temperature; it mathematically can be expressed as,

$$H = \sum_{i=0}^{255} p_i \, log_2 p_i \tag{4}$$

Where, P_i: Probability associated with grey level i.

3.3.4. Energy
Energy is a measure of the homogeneity of an image and is utilized for determining the even degree of a given grey-level deviation of a given texture. In the case of AFM images, as temperature increases, textural deformations are generated, and the image develops inhomogeneity resulting in the reduction of the energy value of an image. Figure 10 represents decreases in energy for temperature increases [32-33].
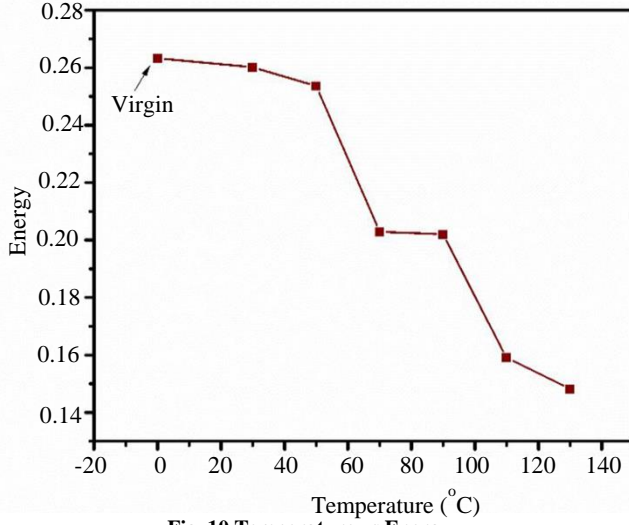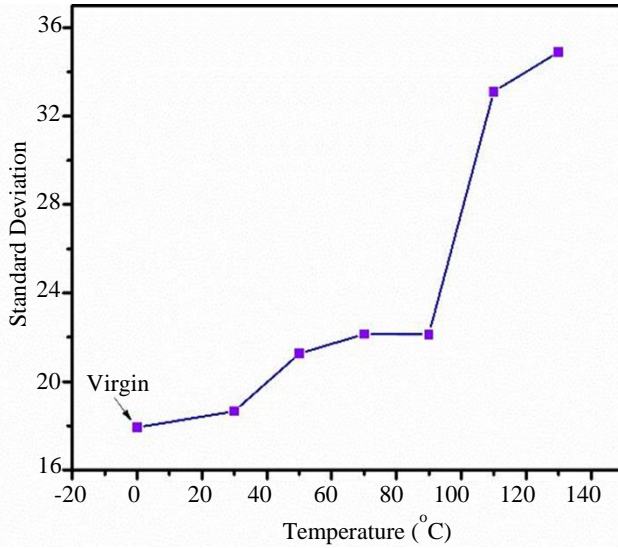
Fig. 10 Temperature vs Energy

Fig. 11 Temperature vs Standard deviation

An angular second moment or energy $= \sum_i \sum_j \{p(i,j)\}^2$ (5)

3.3.5. Standard Deviation

Standard deviation is one of the most significant descriptive statistical methods to measure the deviation of measured values or the data from its mean. It implies a gross measure of the deviation about the target value of light intensity at each such data point. Figure 11 represents the increase in standard deviation, i.e. light intensity increases with temperature.

$$(sd) = \sqrt{\frac{1}{N^2} \sum_{i,j=1}^{N} [p(i,j) - m]^2}$$ (6)

3.3.6. Surface Roughness

The distance between peaks and valleys evaluates Surface roughness [26-27]. Surface roughness using image processing algorithms is represented as,

$$R_a = \frac{1}{M.N.} \sum_{i=1}^{M} \sum_{j=1}^{N} |Z(x_i, y_i) - \mu|$$ (7)

$$\mu = \frac{1}{M.N.} \sum_{i=1}^{M} \sum_{j=1}^{N} |Z(x_i, y_i)|$$ (8)

$$R_q = \sqrt{\frac{1}{M.N.} \sum_{i=1}^{M} \sum_{j=1}^{N} |Z(x_i, y_i) - \mu|^2}$$ (9)

Where,

μ is the arithmetic mean of relative altitude, M and N are the numbers of sampling points in the x and y direction, respectively.

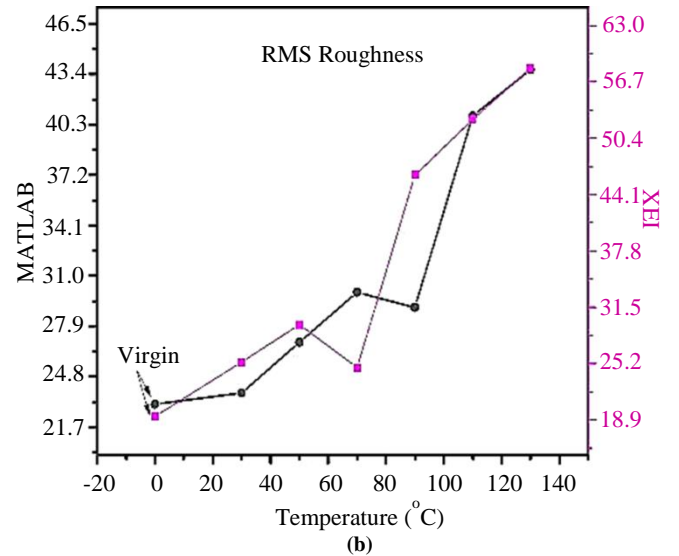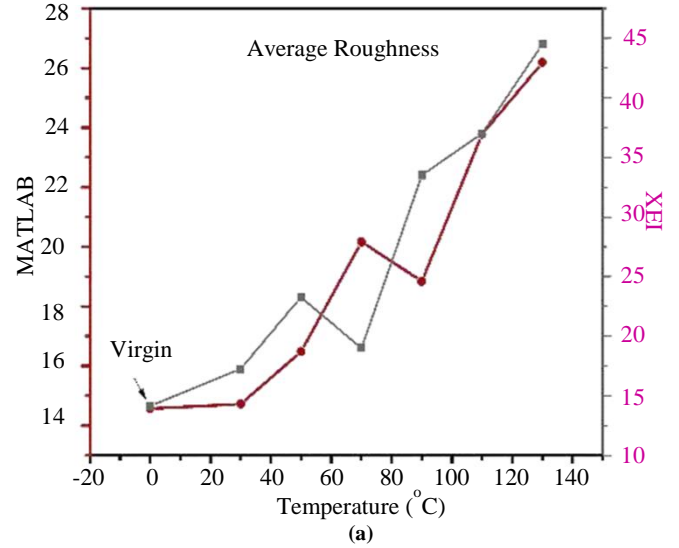$Z(x_i, y_i)$ is the relative altitude of point (x_i, y_i).

(a)

(b)

Fig. 12(a) Temperature vs Average roughness (b) Temperature vs RMS roughness

Figures 12(a) and (b) give a comparative analysis of average and RMS roughness for each sample calculated by XEI software and MATLAB.
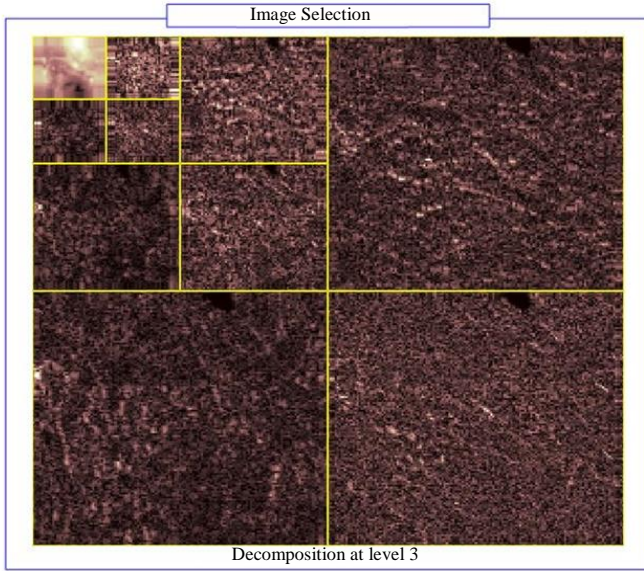
Fig. 13 Three levels of decomposition of the image

compared to CWT and WPT. The following relationship can express the DWT,

$$DTW(p,q) = \sqrt{2^p} \int_{-\infty}^{+\infty} x(t)\Psi^*(2^p t - q)dt \qquad (10)$$

Where ψ is the mother wavelet function, DTW(p,q) are the wavelet coefficients., and ψ* is a complex conjugate of the wavelet function. It decomposes images into Horizontal (H), Vertical (V), and Diagonal (D); detail sub-bands incorporate edges as the image with high-frequency information and the approximation sub-band with low-frequency information. The image decomposition can be achieved by repetitively applying Wavelet Transform to the approximation sub-band.

These images of size 256x256 are wavelets decomposed up to three levels. The decomposition of these images provides a complete representation of changes due to temperature rise.

The availability of many mother wavelets leads to the selection of optimum ones suitable for investigating insulation ageing. In this investigation, the optimum mother wavelet is derived from the minimum value of entropy of wavelet coefficients, as shown in Figure 14. Entropy quantifies information on the content inside the image [32].

Among all, Bior 5.5 displays the most negligible value of entropy magnitude for a particular pattern; hence it is selected as the mother wavelet for further analysis. Wavelet coefficients, Average (ad), Horizontal(hd), Vertical(vd), and Diagonal(dd), are obtained by implementing DWT and three-level decomposition with bior5.5 as the mother wavelet. The graph of the average of all wavelet coefficients Vs temperature for a particular image is shown in Figure 15.
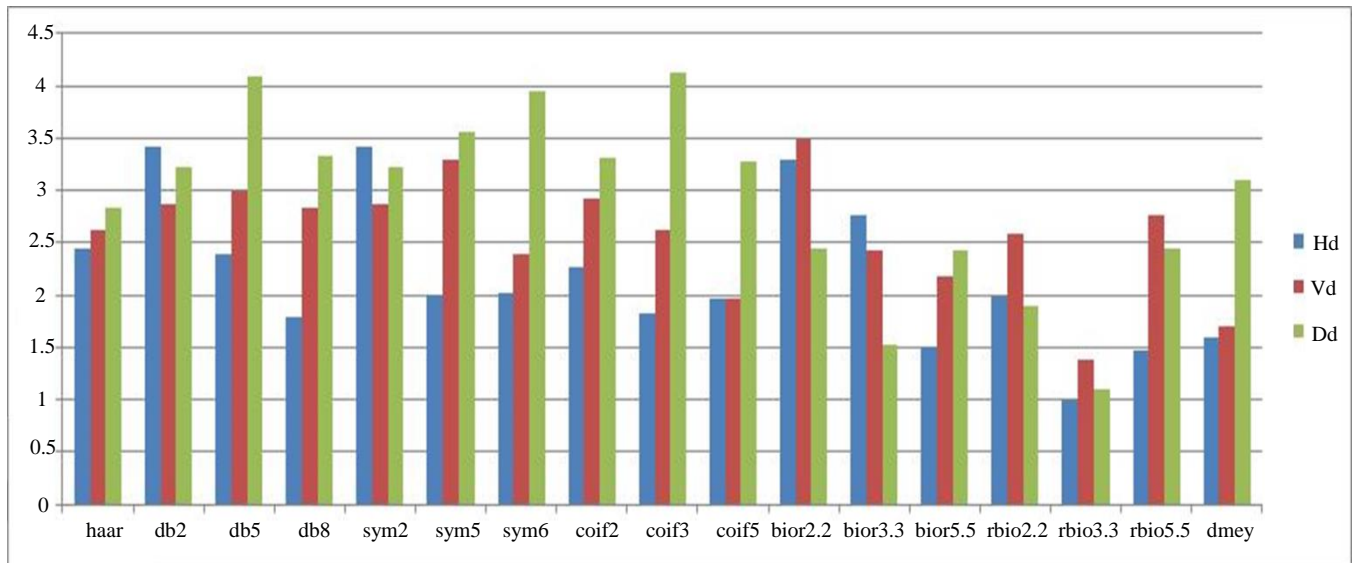
The average roughness increases by 21.96%, 64.56%, 34.37%, 136.91%, 161.66% and 214.71% times under the elevated temperatures of 30, 50, 70, 90, 110 and 130°C respectively, as compared to virgin samples using XEI software. An approximately similar trend was recorded for RMS roughness.

3.3.7. Wavelet Transform Analysis
Wavelet Transform is successfully utilized in various types of image analysis since it provides an arsenal and dynamic toolbox for measuring insulation ageing. Wavelet Transform based multiresolution analysis is superior to being localized in time and frequency. DWT provides adequate information regarding the analysis and synthesis of original images with notable relaxation in computational time

Fig. 14 Magnitude of entropy for various wavelets after three levels of decomposition
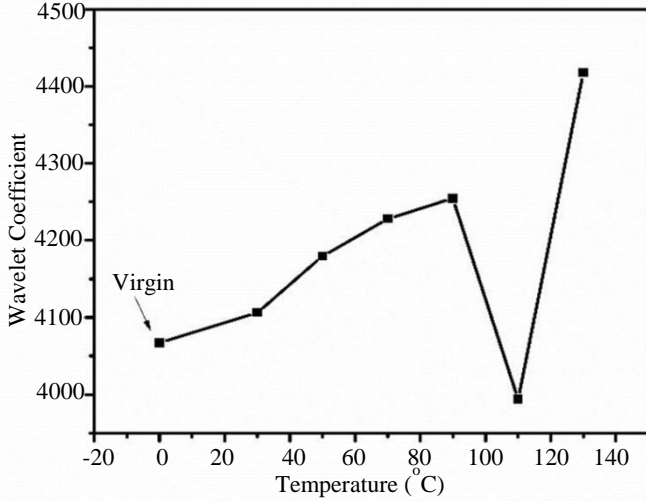
Fig. 15 Temperature vs Wavelet coefficient

4. Analysis Converter Transformer Insulation Degradation using Wavelet Transform

A 315 MVA, 230/123/213 kV single phase dual winding converter transformer's parameters were estimated with the help of ANSYS Maxwell's software [2]. The mathematical model of a single disc of a 123kV valve side winding with five turns per disc is shown in Figure 16. The model is used to identify the analysis of insulation degradation across the single disc in the MATLAB Simulink environment. An impulse of 20kV, 1.2/50µsec is applied, and the FDS data at 50 Hz subjected to 110°C temperature is utilized to analyze the insulation degradation across the turn using wavelet transform.

Figure 17 indicates the neutral current of the converter transformer for various insulation conditions under the application of an impulse of 20kV, 1.2/50µsec.
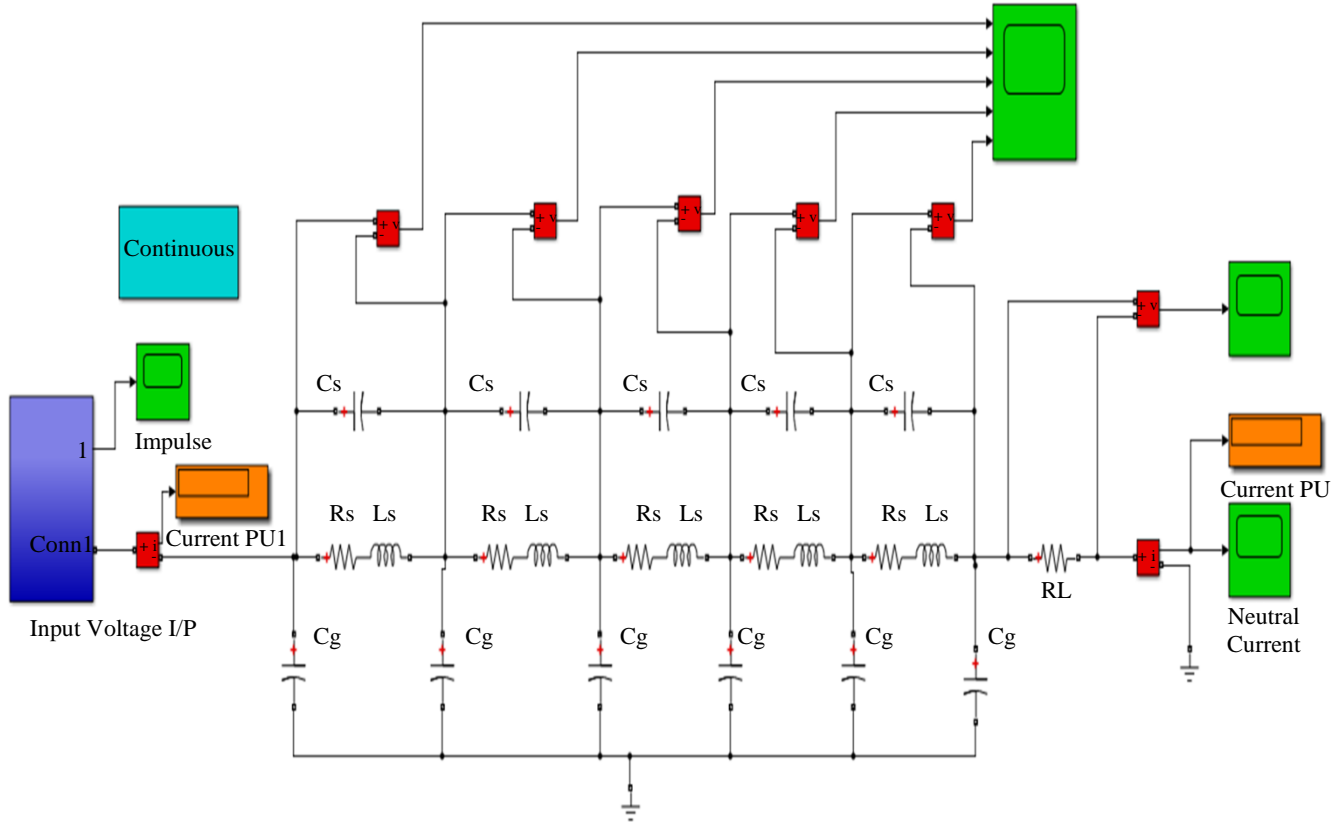

Fig. 16 MATLAB simulink model of single disc of 123 kV valve side winding

A further examination of the neutral current can be analyzed using wavelet transform to determine the failure of the OIP insulation across the winding more effectively. The wavelet transform uses the Daubechies4 wavelet with level 4 (db4) as the mother wavelet and wavelet coefficients, as shown in Figure 18(b). A failure of the OIP insulation causes a typical variation in the energy of the wavelet coefficient for the higher-order frequencies. It is noticed that the decrement of energy of the wavelet coefficient as insulation degradation shifted toward the neutral point, as shown in Figure 19. The change in the energy of the coefficients is found to be 4.54% at the fifth turn compared to the virgin insulation sample.

Thus, the deterioration of the insulation across the winding can be analyzed based on typical changes in the wavelet energy coefficients. It can also determine the approximate localization of the insulation degradation or failure.
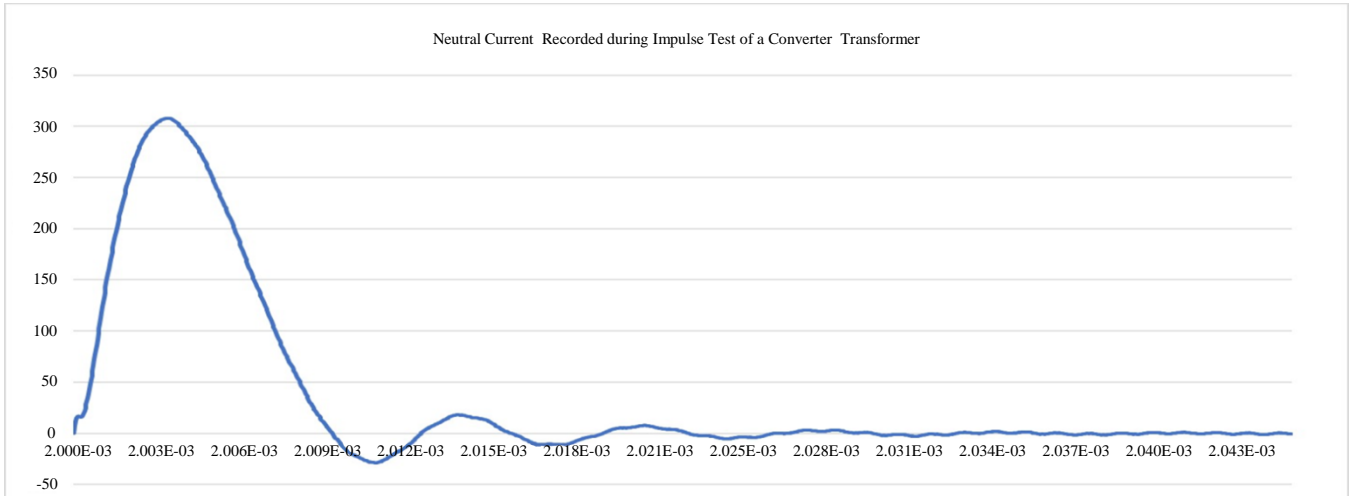
Fig. 17 The neutral current of the converter transformer for various insulation conditions
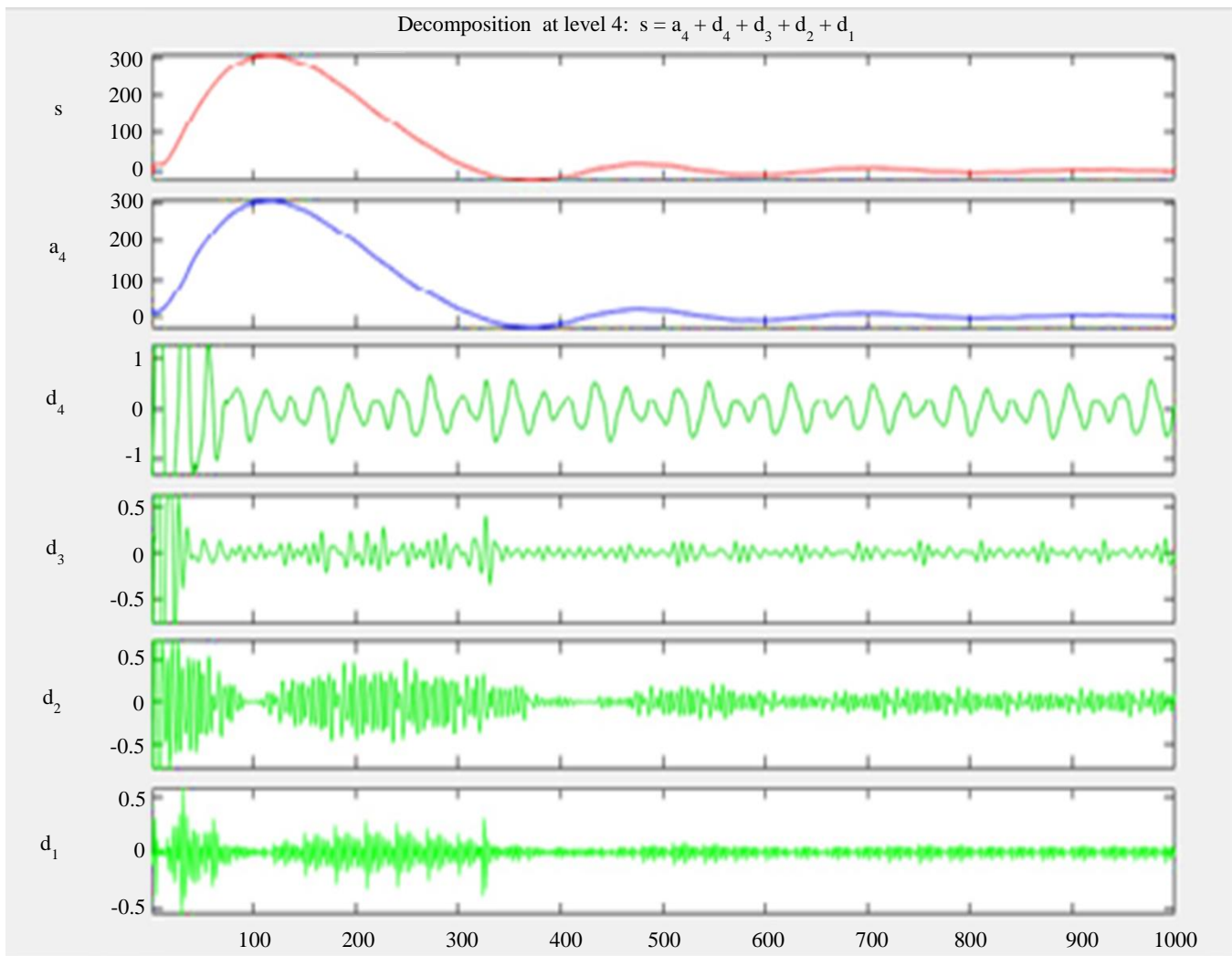

Fig. 18(a) Wavelet transform analysis of neutral current signal (for virgin insulation) using db4 level 4 as mother wavelet
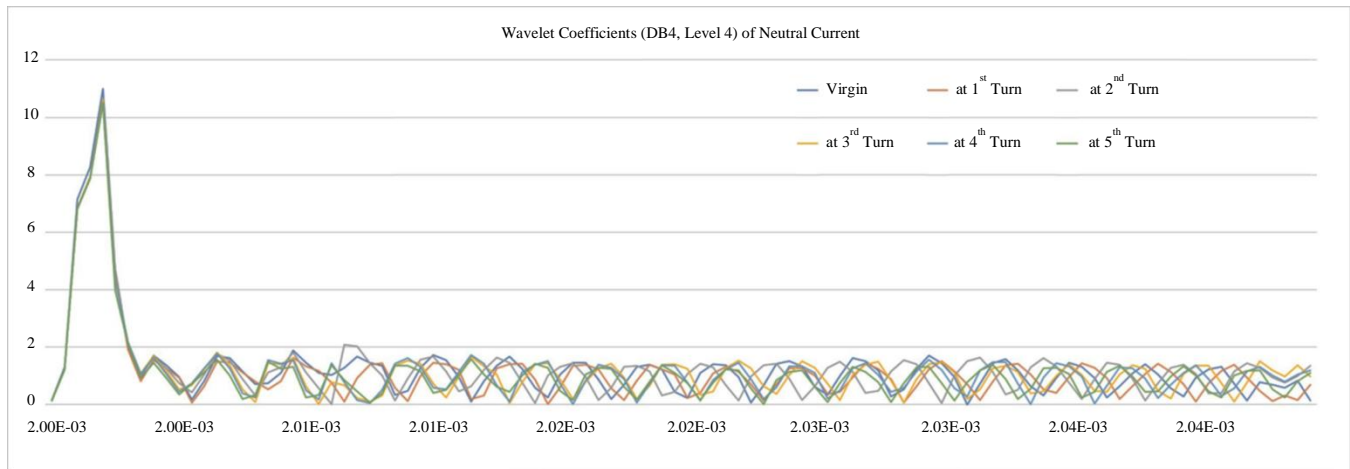
Fig. 18(b) Wavelet transform analysis of neutral current signal for various locations
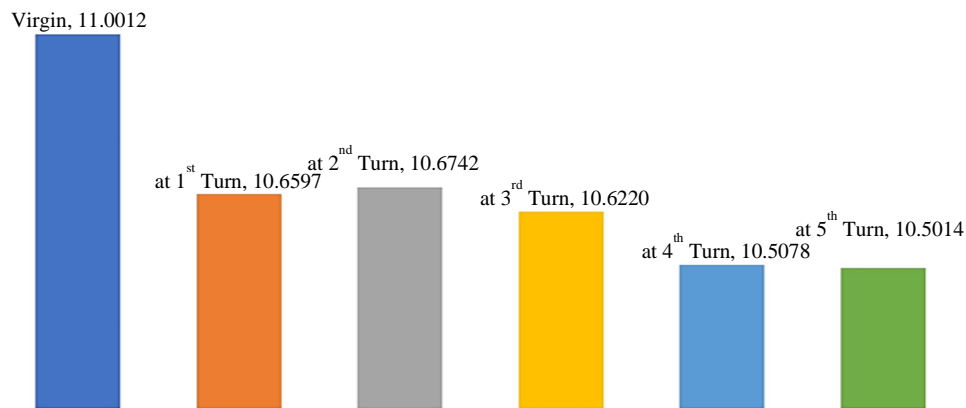

Fig. 19 Energy of the wavelet coefficient for various operating conditions

5. Conclusion

The FDS measurements performed on OIP insulation shows that the insulation performance is greatly affected by a change in frequency and elevated temperature. The relative permittivity, A.C. conductivity, and tanδ significantly change for lower frequency regions. The creations of polar products and cellulose fibre variation are mainly responsible for insulation parameter variation. The FDS measurement also leads to micro-morphological changes inside the structure of OIP insulation. The XEI software has depicted excellent results for morphological changes. The RMS surface roughness varied from 21.96% to 214.7% for elevated temperatures between 30°C to 130°C.

The experimental results suggest that the average RMS roughness, energy, and entropy in the spatial domain are effective methods in the degradation assessment of OIP samples. The horizontal, vertical, and diagonal detail wavelet entropy coefficients are determined by implementing Discrete Wavelet Transform (DWT).

The statistical parameter, such as the average wavelet coefficient, is extracted using bior5.5 as the mother wavelet after performing three-level decomposition. The extracted parameters in the spatial and frequency domain confirm insulation degradation. Finally, one disk, five turns single phase dual winding converter transformer modelled in MATLAB Simulink environment and tested under impulse condition. The neutral current for various insulation conditions is captured, and the wavelet coefficient energy is utilized for the insulation degradation. The energy of the coefficients is inherently decreasing, and 4.54% changes in the energy coefficients when the insulation at 5th turn is degraded compared to the virgin sample. Thus, the FDS method is beneficial for the analysis of insulation degradation in the winding of the converter transformer.

Acknowledgements

References

[1] Susilo et al., "Study on Dissolved Gas Due Tue Thermally Degraded Insulating Paper in Transformer Oil," *Procedia Technology*, vol. 11, pp. 257-262, 2013. [CrossRef] [Google Scholar] [Publisher Link]

[2] Shrikant S. Mopari, "Estimation of Inductance and Capacitance Parameters of Single Phase Dual Winding Converter Transformer with FEM," *IEEE 11th International Conference on Communication Systems and Network Technologies (CSNT)*, Indore, India, pp. 83-88, 2022. [CrossRef] [Google Scholar] [Publisher Link]

[3] G. M. Urbani, and R. S. Brooks, "Using the Recovery Voltage Method to Evaluate Aging in Oil-Paper Insulation," *In Proceedings of the 1998 IEEE 6th International Conference on Conduction and Breakdown in Solid Dielectrics (Cat. No.98CH36132)*, Vasteras, Sweden, pp. 93-97, 1998. [CrossRef] [Google Scholar] [Publisher Link]

[4] T. K. Saha, "Review of Modern Diagnostic Techniques for Assessing Insulation Condition in Aged Transformers," *IEEE Transactions on Dielectrics and Electrical Insulation*, vol. 10, no. 5, pp. 903-917, 2003. [CrossRef] [Google Scholar] [Publisher Link]

[5] T. K. Saha, and P. Purkait, "Investigation of Polarization and Depolarization Current Measurements for the Assessment of Oil-Paper Insulation of Aged Transformers," *IEEE Transactions on Dielectrics and Electrical Insulation*, vol. 11, no. 1, pp. 144-154, 2004. [CrossRef] [Google Scholar] [Publisher Link]

[6] J. H. Yew, T. K. Saha, and A. J. Thomas, "Impact of Temperature on the Frequency Domain Dielectric Spectroscopy for the Diagnosis of Power Transformer Insulation," *IEEE Power Engineering Society General Meeting, Montreal,* QC, Canada, p. 7, 2006. [CrossRef] [Google Scholar] [Publisher Link]

[7] Shi-Qiang Wang et al., "Investigation on Dielectric Response Characteristics of Thermally Aged Insulating Pressboard in Vacuum and Oil-Impregnated Ambient," *IEEE Transactions on Dielectrics and Electrical Insulation*, vol. 17, no. 6, pp. 1853–1862, 2010. [CrossRef] [Google Scholar] [Publisher Link]

[8] A. Setayeshmehr et al., "Dielectric Spectroscopic Measurements on Transformer Oil-Paper Insulation under Controlled Laboratory Conditions," *IEEE Transactions on Dielectrics and Electrical Insulation*, vol. 15, no. 4, pp. 1100-1111, 2008. [CrossRef] [Google Scholar] [Publisher Link]

[9] Quanmin Dai et al., "Temperature Segment Compensation Method of Dissipation Factor for Insulation Diagnosis in Converter Transformer Bushing," *IEEE Access*, vol. 10, pp. 10310-10316, 2022. [CrossRef] [Google Scholar] [Publisher Link]

[10] Ruijin Liao et al., "A Comparative Study of Physicochemical, Dielectric and Thermal Properties of Pressboard Insulation Impregnated with Natural Ester and Mineral Oil," *IEEE Transactions on Dielectrics and Electrical Insulation*, vol. 18, no. 5, pp. 1626-1637, 2011. [CrossRef] [Google Scholar] [Publisher Link]

[11] M. K. Pradhan, and K. J. H. Yew, "Experimental Investigation of Insulation Parameters Affecting Power Transformer Condition Assessment using Frequency Domain Spectroscopy," *IEEE Transactions on Dielectrics and Electrical Insulation*, vol. 19, no. 6, pp. 1851-1859, 2012. [CrossRef] [Google Scholar] [Publisher Link]

[12] Ruijin Liao et al., "Quantitative Analysis of Ageing Condition of Oil-Paper Insulation by Frequency Domain Spectroscopy," *IEEE Transactions on Dielectrics and Electrical Insulation*, vol. 19, no. 3, pp. 821-830, 2012. [CrossRef] [Google Scholar] [Publisher Link]

[13] R. Setnescu et al., "Thermal Lifetime of Cellulose Insulation Material Evaluated by an Activation Energy based Method," *Cellulose*, vol. 21, no. 1, pp. 823–833, 2014. [CrossRef] [Google Scholar] [Publisher Link]

[14] E. I. Koufakis, C. G. Karagiannopoulos, and P. D. Bourkas, "Thermal Coefficient Measurements of the Insulation in Distribution Transformers of a 20KV Network," *Measurement*, vol. 41, no. 1, pp. 10–19, 2008. [CrossRef] [Google Scholar] [Publisher Link]

[15] P. E. Sánchez-Jiménez et al., "An Improved Model for the Kinetic Description of the Thermal Degradation of Cellulose," *Cellulose*, vol. 18, no. 6, pp. 1487–1498, 2011. [CrossRef] [Google Scholar] [Publisher Link]

[16] Muhammad Aslam et al., "Health Analysis of Transformer Winding Insulation through Thermal Monitoring and Fast Fourier Transform (FFT) Power Spectrum," *IEEE Access*, vol. 9, pp. 114207-114217, 2021. [CrossRef] [Google Scholar] [Publisher Link]

[17] J. H. Yew, M. K. Pradhan, and T. K. Saha, "Effects of Moisture and Temperature on the Frequency Domain Spectroscopy Analysis of Power Transformer Insulation," *2008 IEEE Power and Energy Society General Meeting - Conversion and Delivery of Electrical Energy in the 21st Century*, Pittsburgh, PA, USA, pp. 1-8, 2008. [CrossRef] [Google Scholar] [Publisher Link]

[18] Raj B. Jadav, Chandima Ekanayake, and Tapan K. Saha, "Impact of Moisture and Ageing on the Dielectric Response of Transformer Insulation," *22nd Australasian Universities Power Engineering Conference (AUPEC)*, Bali, Indonesia, pp. 1-6, 2012. [Google Scholar] [Publisher Link]

[19] Raj B. Jadav, Chandima Ekanayake, and Tapan K. Saha, "Understanding the Impact of Moisture and Ageing of Transformer Insulation on Frequency Domain Spectroscopy," *IEEE Transactions on Dielectrics and Electrical Insulation*, vol. 21, no. 1, pp. 369-379, 2014. [CrossRef] [Google Scholar] [Publisher Link]

[20] Omar Noureldeen, "Effect of Geometrical Arrangement of Power Transformer Insulation and Its Temperature on Dielectric Response Measurements," *Journal of Engineering Sciences*, vol. 35, no. 6, pp. 1455–1465, 2007. [CrossRef] [Google Scholar] [Publisher Link]

[21] Ruijin Liao et al., "Quantitative Analysis of Insulation Condition of Oil-Paper Insulation based on Frequency Domain Spectroscopy," *IEEE Transactions on Dielectrics and Electrical Insulation*, vol. 22, no. 1, pp. 322-334, 2015. [CrossRef] [Google Scholar] [Publisher Link]

[22] Youyuan Wang et al., "Investigation of Characteristic Parameters for Condition Evaluation of Transformer Oil-Paper Insulation using Frequency Domain Spectroscopy," *International Transactions on Electrical Energy Systems*, vol. 25, no. 11, pp. 2921-2932, 2015. [CrossRef] [Google Scholar] [Publisher Link]

[23] Rui-Jin Liao, Chao Tang, and Li-Jun Yang, "Study on the Microscopic Figures of Power Transformer Insulation Paper under Electrical and Thermal Stresses," *International Journal of Modern Physics B*, vol. 22, no. 20, pp. 3397–3403, 2008. [CrossRef] [Google Scholar] [Publisher Link]

[24] Rui-jin Liao et al., "Thermal Aging Micro-Scale Analysis of Power Transformer Pressboard," *IEEE Transactions on Dielectrics and Electrical Insulation*, vol. 15, no. 5, pp. 1281-1287, 2008. [CrossRef] [Google Scholar] [Publisher Link]

[25] Potao Sun et al., "Accumulative Effect of Oil-Paper Insulation System under Multiple Lightning Impulse Voltage," *2013 Annual Report Conference on Electrical Insulation and Dielectric Phenomena*, Chenzhen, China, pp. 202-205, 2013. [CrossRef] [Google Scholar] [Publisher Link]

[26] Wenxia Sima et al., "Study on the Accumulative Effect of Repeated Lightning Impulses on Insulation Characteristics of Transformer Oil Impregnated Paper," *IEEE Transactions on Dielectrics and Electrical Insulation*, vol. 21, no. 4, pp. 1933-1941, 2014. [CrossRef] [Google Scholar] [Publisher Link]

[27] Chenmeng Zhang, Shijun Xie, and Yu Zhang, "Repeated Impulse Aging of Oil-Polypropylene Insulation," *IEEE Transactions on Dielectrics and Electrical Insulation*, vol. 26, no. 5, pp. 1581-1587, 2019. [CrossRef] [Google Scholar] [Publisher Link]

[28] Qingpeng Wang et al., "Study of Insulation Material Properties Subjected to Nonlinear AC–DC Composite Electric Field for Converter Transformer," *IEEE Transactions on Magnetics*, vol. 55, no. 2, pp. 1-4, 2019. [CrossRef] [Google Scholar] [Publisher Link]

[29] Huize Cui et al., "A Comprehensive Analyses of Aging Characteristics of Oil-Paper Insulation System in HVDC Converter Transformers," *IEEE Transactions on Dielectrics and Electrical Insulation*, vol. 27, no. 5, pp. 1707-1714, 2020. [CrossRef] [Google Scholar] [Publisher Link]

[30] Osvaldo A. Rosso et al., "Wavelet Entropy: A New Tool for Analysis of Short Duration Brain Electrical Signals," *Journal of Neuroscience Methods*, vol. 105, no. 1, pp. 65-75, 2001. [CrossRef] [Google Scholar] [Publisher Link]

[31] Shuaibing Li et al., "Aging Feature Extraction of Oil-Impregnated Insulating Paper using Image Texture Analysis," *IEEE Transactions on Dielectrics and Electrical Insulation*, vol. 24, no. 3, pp. 1636-1645, 2017. [CrossRef] [Google Scholar] [Publisher Link]

[32] Praveen Kumar Gandla et al., "Evaluation of Surface Roughness in Incremental Forming using Image Processing-based Methods," *Measurement*, vol. 164, p. 108055, 2020. [CrossRef] [Google Scholar] [Publisher Link]

[33] Nathan D. Jacob, Behzad Kordi, and Sherif S. Sherif, "Assessment of Power Transformer Paper Ageing using Wavelet Texture Analysis of Microscopy Images," *IEEE Transactions on Dielectrics and Electrical Insulation*, vol. 27, no. 6, pp. 1898-1905, 2020. [CrossRef] [Google Scholar] [Publisher Link]

[34] T. K. Saha, and Zheng Tong Yao, "Experience with Return Voltage Measurements for Assessing Insulation Conditions in Service-Aged Transformers," *IEEE Transactions on Power Delivery*, vol. 18, no. 1, pp. 128-135, 2003. [CrossRef] [Google Scholar] [Publisher Link]

[35] Pannala Krishna Murthy et al., "Wavelet Transform Approach for Detection and Location of Faults in HVDC System," *IEEE Region 10 and the 3rd International Conference on Industrial and Information Systems*, pp. 1-6, 2008. [CrossRef] [Google Scholar] [Publisher Link]

[36] Hongchun Shu, Xincui Tian, and Yuetao Dai, "The Identification of Internal and External Faults for ±800kV UHVDC Transmission Line based on S-Transform of the Polarity Wave," *3rd International Congress on Image and Signal Processing*, Yantai, China, pp. 3060-3063, 2010. [CrossRef] [Google Scholar] [Publisher Link]

[37] Hongchun Shu, Xincui Tian, and Yuetao Dai, "The Identification of Internal and External Faults for ±800kV UHVDC Transmission Line based on using Wavelet based Multi-Resolution Analysis," *2nd International Workshop on Database Technology and Applications*, Wuhan, China, pp. 1-4, 2010. [CrossRef] [Google Scholar] [Publisher Link]

[38] Luhua Xing et al., "A New Protection Principle for HVDC Transmission Lines Based on Fault Component of Voltage and Current," *2011 IEEE Power and Energy Society General Meeting*, Detroit, USA, pp. 1-6, 2011. [CrossRef] [Google Scholar] [Publisher Link]

[39] Anjali Soni, and Prashant Jain, "Iris Recognition using Four Level HAAR Wavelet Transform: A Literature Review," *SSRG International Journal of Electronics and Communication Engineering*, vol. 3, no. 6, pp. 14-18, 2016. [CrossRef] [Google Scholar] [Publisher Link]

[40] S. Chandra Shekar, G. Ravi Kumar, and S. V. N. L. Lalitha, "A Transient Current based Micro-Grid Connected Power System Protection Scheme using Wavelet Approach," *International Journal of Electrical and Computer Engineering (IJECE)*, vol. 9, no. 1, pp. 14-22, 2019. [CrossRef] [Google Scholar] [Publisher Link]

[41] Mahmood Parsi et al., "Wavelet based Fault Location on Power Transmission Lines using Real-World Travelling Wave Data," *Electric Power Systems Research*, vol. 186, p. 106261, 2020. [CrossRef] [Google Scholar] [Publisher Link]

[42] Pathomthat Chiradeja, and Atthapol Ngaopitakkul, "Winding-to-Ground Fault Location in Power Transformer Windings using Combination of Discrete Wavelet Transform and Back-Propagation Neural Network," *Scientific Reports*, vol. 12, pp. 1-14, 2022. [CrossRef] [Google Scholar] [Publisher Link]

[43] Shrikant Mopari et al., "Evaluation of Oil Impregnated Paper Insulation for Converter Transformer under FDS," *3rd International Conference ICKE-2023*, Aurangabad, India, 2023.